Quantum Dispersion in Mono-layer Graphene using Wave Packets and Rashba Spin-Orbit Interaction

Eduardo Serna*
Centro de Investigación en Ciencias, Universidad Autónoma del Estado de Morelos, Morelos, 62209, México

I. Rodríguez Vargas†
Unidad Académica de Física, Universidad Autónoma de Zacatecas, Zacatecas, 98060, México

L. Diago-Cisneros‡
Facultad de Física, Universidad de La Habana, La Habana, 10400, Cuba
(Dated: June 26, 2025)

This paper presents a theoretical and computational study on the impact of Rashba spin-orbit interaction (SOIR) on electron transmission through a potential barrier in monolayer graphene. The energy dispersion relations were numerically obtained via the finite differences method applied to the Schrödinger equation, using a model Hamiltonian incorporating graphene, SOIR, and a potential barrier. Our findings reveal that the presence of SOIR significantly modifies the electron transmission coefficients compared with pristine graphene conditions. While electron transmission in pristine graphene remains near unity with minor reductions due to quantum interference effects in a Gaussian wave packet, introducing SOIR leads to intricate transmission patterns dependent on the barrier parameters and wave packet characteristics. These effects arise from phenomena such as spin degeneracy lifting and spin-dependent scattering mechanisms. The results emphasize the critical role that SOIR plays in engineering sophisticated quantum devices, offering potential applications in spintronic technologies and quantum computing.

I. INTRODUCTION

La dispersión cuántica en grafeno, entendida como la relación entre niveles de energía y sus respectivos vectores de onda, es esencial para explicar las sobresalientes propiedades electrónicas y de transporte observadas en este material bidimensional único. Su estructura de red hexagonal genera fermiones de Dirac sin masa, lo que origina particulares fenómenos cuánticos como movilidad extremadamente alta, transporte balístico en escalas micrométricas, y ausencia intrínseca de banda prohibida[**?**]. Dentro de estos fenómenos, resulta especialmente interesante estudiar el papel de la SOIR, que puede modificar significativamente el comportamiento electrónico y conducir a efectos novedosos de interferencia y dispersión relacionados con el espín electrónico.

La comprensión precisa de estas interacciones es crítica no solamente desde la perspectiva teórica, sino que además representa la base fundamental para aplicaciones tecnológicas emergentes en áreas estratégicas tales como la spintrónica y la computación cuántica[**?** **?** **?**]. En este contexto, la ecuación de Schrödinger provee el marco fundamental para analizar el transporte electrónico, siendo particularmente idónea su solución numérica mediante métodos robustos como la técnica de diferencias finitas (FDM). Consecuentemente, el objetivo central de este trabajo es calcular detalladamente las relaciones de dispersión energética para electrones en grafeno monocapa bajo interacción SOIR utilizando paquetes de onda gaussianos, destacando cómo estos efectos cuánticos pueden ser explotados para la ingeniería avanzada de dispositivos nanotecnológicos especializados en aplicaciones spintrónicas y de información cuántica.

Finalmente, cabe destacar que uno de los aspectos esenciales abordados en este trabajo radica en la formulación analítica precisa del vector corriente, cuya expresión analítica es dada por la ecuación(35). Esta expresión representa un pilar fundamental para comprender detalladamente los efectos y mecanismos subyacentes en los fenómenos de transporte electrónico en presencia de SOIR. Por ello, la obtención y análisis de dicha ecuación constituye una aportación significativa al campo, especialmente en aplicaciones relacionadas con dispositivos spintrónicos y tecnologías cuánticas emergentes.

A. Klein Paradox

Applying an electrostatic potential to graphene can create regions where electrons are classically forbidden due to energy constraints[**?**]. For instance, a negative gate voltage can shift the Fermi level into the valence band, establishing a potential barrier that electrons do not have sufficient energy to overcome, according to classical physics[**?**]. However, in graphene, electron transmission through such barriers can exhibit unusual behavior due to the Klein paradox.

The Klein paradox describes the phenomenon where electrons in graphene can tunnel through electrostatic potential barriers with a probability approaching unity, even at perpendicular incidence, seemingly defying the

* sernaed95@gmail.com
† isaac@fisica.uaz.edu.mx
‡ ldiago@fisica.uh.cu

principles of classical mechanics[**?**]. This counterintuitive transmission arises from the relativistic nature of electrons in graphene, where, within the barrier region, incident electrons can be converted into holes, allowing for unimpeded passage[**?**]. The Klein paradox is a direct consequence of graphene's unique linear dispersion relation and the associated massless Dirac fermion behavior. While this perfect transmission through barriers might pose challenges for achieving electron confinement in some device designs, it also presents opportunities for developing novel tunneling-based electronic devices. Beyond simply creating a forbidden region, the application of electrostatic potential can dramatically alter electron transmission through various other mechanisms, influencing the refractive index and leading to phenomena like electron lensing[**?**].

B. Rashba-Type Spin-Orbit Interaction

SOIR is a relativistic effect that arises in systems lacking structural inversion symmetry[**?**]. La SOIR es especialmente relevante debido a su capacidad para modificar significativamente la estructura electrónica del grafeno, induciendo acoplamientos particulares entre el espín y el momento de los electrones. Esto lleva a exhibir fenómenos emergentes tales como la interferencia cuántica dependiente del espín y efectos de dispersión no convencionales. El impacto de la SOIR no solo aporta nuevas perspectivas en física fundamental, sino que también abre posibilidades prometedoras para aplicaciones avanzadas en tecnologías spintrónicas y dispositivos basados en información cuántica.

In graphene, SOIR can be induced by an external electric field applied perpendicular to the graphene plane or through proximity to a substrate[**?**]. A key consequence of SOIR is the breaking of spin degeneracy, where the energy levels of electrons with opposite spins are no longer the same, even in the absence of an external magnetic field[**?**]. Controlling spin degeneracy through electric fields via SOIR is particularly valuable for spintronic applications. It enables electron spin manipulation without depending on magnetic fields, which typically require more power and are challenging to incorporate effectively into nanoscale systems.

Furthermore, SOIR modifies the effective mass of charge carriers in graphene[**?**]. It can lead to the opening of an energy gap at the Dirac points, effectively giving the otherwise massless Dirac fermions a finite mass. In systems with strong spin-orbit coupling, such as certain heavy-hole systems, specific types of SOIR (like k^3-Rashba spin-orbit coupling) can even result in anisotropic band structures and the emergence of additional spin-degeneracy points under light illumination. While this specific example refers to heavy holes, the principle that SOIR can significantly alter the band structure and effective mass of carriers is relevant to graphene, particularly when considering proximity-induced effects from substrates with strong spin-orbit coupling[**?**]. The modification of the effective mass by SOIR can profoundly impact graphene's transport properties, influencing carrier mobility and the density of states. Notably, tuning the strength of SOIR in graphene can even induce a transition from the Klein tunneling regime (perfect transmission) to the anti-Klein tunneling regime (perfect reflection) when electrons encounter a potential barrier. This ability to control the transmission probability through potential barriers using SOIR opens up exciting possibilities for creating novel electronic devices that leverage this fundamental quantum mechanical phenomenon[**?**].

En la próxima sección, se describirá detalladamente el modelo físico-matemático adoptado en este estudio. Partiendo de la base conceptual presentada anteriormente sobre la dispersión cuántica y la interacción espín-órbita tipo Rashba, se definirá el sistema y las ecuaciones correspondientes que permiten simular numéricamente los fenómenos observados en nuestros resultados.

II. DEVELOPMENT

A. Physical Model

A quantum channel was fabricated using a hexagonal boron nitride substrate, upon which monolayer graphene (MLG) was deposited and subsequently capped with a silicon dioxide layer. Two metallic electrodes were incorporated to generate a perpendicular electric field, thereby confining a Gaussian wave packet (GWP) within the graphene. We also added a rectangular electrostatic potential barrier, where we incorporate the SOIR. The system is more deeply explained in our previous article[**?**]

B. Mathematical Model

From the physical model, we can get a mathematical model which describes the temporal evolution and consequently the quantum dispersion of the fDs in the MLG.

Starting with the pristine graphene hamiltonian[**?**]:

$$\hat{\boldsymbol{H}}_G = v_{\text{F}}\vec{\sigma}\cdot\vec{p}, \tag{1}$$

With $\vec{\sigma} = \hat{\sigma}_x\hat{\imath} + \hat{\sigma}_y\hat{\jmath}$, being the pseudospin Pauli matrices $\hat{\sigma}_x = \left(\begin{smallmatrix} 0 & 1 \\ 1 & 0 \end{smallmatrix}\right)$, $\hat{\sigma}_y = \left(\begin{smallmatrix} 0 & -i \\ i & 0 \end{smallmatrix}\right)$, and $\vec{p} = \hat{p}_x\hat{\imath} + \hat{p}_y\hat{\jmath}$, the momentum operator, which x, y components read $\hat{p}_x = -i\hbar\frac{\partial}{\partial x}$ and $\hat{p}_y = -i\hbar\frac{\partial}{\partial y}$, respectively. From this point forward, v_{F} stands for the Fermi velocity of the carriers in MLG, which satisfies

$$v_{\text{F}} \approx \frac{c}{300}. \tag{2}$$

The previous hamiltonian can be rewritten as:

$$\hat{\boldsymbol{H}}_G = -i\hbar v_{\mathrm{F}} \begin{pmatrix} 0 & \frac{\partial}{\partial x} - i\frac{\partial}{\partial y} \\ \frac{\partial}{\partial x} + i\frac{\partial}{\partial y} & 0 \end{pmatrix}. \tag{3}$$

Assuming that the momentum-dependent term of the Rashba Hamiltonian for Q1D (quasi-one dimensional) semiconductor hetero-structures can be extended to the context of MLG-Q1D[**? ? ?**], it follows that the hamiltonian for the SOIR can be written as:

$$\hat{\boldsymbol{H}}_R = \begin{pmatrix} 0 & k_{\alpha-} + k_{\beta-} \\ k_{\alpha+} + k_{\beta+} & 0 \end{pmatrix}, \tag{4}$$

Where $k_{\alpha\pm} = \alpha\left(k_{\pm}^2/k_{\mp}\right)$ and $k_{\beta\pm} = \beta k_{\pm}^3$; also defining that $k_{\pm} = k_x \pm ik_y$ which are the initial wave numbers of the system. The symbols α and β represent the linear and cubic contribution of the SOIR respectively.

To calculate the values of the coupling constants α and β, we base our approach on the equations proposed by Wong and Mireles[**?**]:

$$\alpha = \frac{eE_bP^2}{3E_i\left(E_i + E_g\right)} \tag{5}$$

$$\beta = -\frac{eE_bP^2\left(2E_i + E_g\right)}{3E_i\left(E_i + E_g\right)^2 k_c^2} \tag{6}$$

$$E_i = \frac{2P^2k_c^2}{3E_g} \tag{7}$$

$$\frac{2P^2}{m_0E_g} = \frac{m_0}{m^*} - 1 \tag{8}$$

$$E_b = \frac{V_b}{el} \tag{9}$$

where e is the charge of heavy holes in the potential barrier region, P is the momentum of the charge carriers, E_g is the energy of the band gap, k_c is a critical wave number that satisfies the condition $k \ll k_c$, m_0 is the free electron mass, m^* is the effective mass of charge carriers in the potential barrier region, V_b is the height of the barrier, and l is the width of the barrier.

Based on previous experimental data ([**? ? ?**]), we define, as a test, $E_g = 0.03$ eV and $m^* = 0.47m_0$; while we define a value for the critical wave number $k_c = 0.2$ Å^{-1} that coincides with experimentally obtained values.

If we substitute these numerical values, we can use (8) to obtain $P^2 = 1.54 \times 10^{-32}$ kg·eV; and, therefore, $E_i = 1.37 \times 10^{-32}$ eV.

Finally, we define the width and height of the barrier based on different physical models already presented in the literature.

Using these numerical results, we can find α and β. For example, if $l = 100$ Å and $V_b = 0.5$ eV, then $\alpha = 0.25$ eV·Å and $\beta = -1.56$ eV·Å.

For this research, we assume the heavy holes only in the region defined by the potential barrier.

The potential barrier is defined only in the specified region.

With the following hamiltonian:

$$\hat{\boldsymbol{H}}_V = \boldsymbol{I}_2 V(x) \tag{10}$$

Adding up the graphene(3), the SOIR(4), and the potential barrier(10) Hamiltonians, while also zeroing the parameters in the y direction, we get:

$$\hat{\boldsymbol{H}} = \begin{pmatrix} V(x) & (k_{\alpha-} + k_{\beta-}) - i\hbar v_{\mathrm{F}}\frac{\partial}{\partial x} \\ (k_{\alpha+} + k_{\beta+}) - i\hbar v_{\mathrm{F}}\frac{\partial}{\partial x} & V(x) \end{pmatrix}. \tag{11}$$

Note that if we wanted to see the results in the y direction, we would have to zero the partial derivatives of x.

C. Finite differences scheme

The main equation to solve is the time-dependent Schrödinger equation:

$$i\hbar\frac{d}{dt}\boldsymbol{\Psi}(x,t) = \hat{\boldsymbol{H}}\boldsymbol{\Psi}(x,t) \tag{12}$$

In our case, we consider a Gaussian wave packet (GWP) for each component of the pseudospinor $\boldsymbol{\Psi}(x,t) = \begin{pmatrix} \psi_A(x,t) \\ \psi_B(x,t) \end{pmatrix}$. The GWP at an initial time has the following form:

$$\psi_j(x,t_0) = \frac{\xi_j}{\sqrt[4]{\pi\sigma^2}} e^{-\frac{(x-x_0)^2}{2\sigma^2}} e^{ixk_0} \tag{13}$$

Where ξ is the initial configuration of the pseudospinor, k_0 is the initial wave number in x, and the subscript j indicates the component being used.

For the development of this article, we are using the following pseudospinor configuration options:

$$\xi = \begin{pmatrix} 1 \\ 0 \end{pmatrix}, \begin{pmatrix} 1 \\ 1 \end{pmatrix}, \begin{pmatrix} 1 \\ i \end{pmatrix}, \begin{pmatrix} 1 \\ e^{i\pi/4} \end{pmatrix}. \tag{14}$$

The wave packet is then defined as follows:

$$\boldsymbol{\Psi}(x,0) = \frac{1}{\sqrt{\xi_A^2 + \xi_B^2}} \begin{pmatrix} \psi_A \\ \psi_B \end{pmatrix} \tag{15}$$

For the probability density calculated below, we use the following definition:

$$\rho(x,t) = |\boldsymbol{\Psi}|^2 = |\psi_A|^2 + |\psi_B|^2 \tag{16}$$

D. Temporal Evolution Operator

To solve the Schrödinger equation(12), we propose using a temporal evolution operator (TEO), based on the following equation:

$$\boldsymbol{\Psi}(x,t) = \hat{U}(t,t_0)\boldsymbol{\Psi}(x,t_0) \tag{17}$$

We can see that by applying the operator, we obtain a time t from an initial time t_0. If we substitute the TEO equation(17) into the Schrödinger equation(12), we can develop the algebra and solve the differential equation to obtain the TEO. Since the Hamiltonian does not depend on time, we can rewrite eq.(17) as:

$$\boldsymbol{\Psi}(x,t) = e^{-\frac{i\delta t}{\hbar}\hat{\boldsymbol{H}}}\boldsymbol{\Psi}(x,t_0) \tag{18}$$

Where δt is the time step that we will discretize later. The previous exponential can be approximated through the first-order Taylor series as:

$$e^{-\frac{i\delta t}{\hbar}\hat{\boldsymbol{H}}} = \frac{2}{\boldsymbol{I} + \frac{i\delta t}{2\hbar}\hat{\boldsymbol{H}}} - \boldsymbol{I} \tag{19}$$

Using a change of variable, we can rewrite the previous equation(19) as:

$$\boldsymbol{\Phi}(x,t_0) + \frac{i\delta t}{2\hbar}\hat{\boldsymbol{H}}\boldsymbol{\Phi}(x,t_0) = 2\boldsymbol{\Psi}(x,t_0) \tag{20}$$

This equation represents a system of 2×2 equations (since we have two unknowns, ϕ_A and ϕ_B, and when developing the matrix, we can see that two equations are formed).

Since both equations have derivatives, we use the finite difference method to solve both equations for the entire space simultaneously. To do this, we first discretize the system of equations(20) along the entire space j from 0 to J.

To maintain the stability of the numerical analysis in the finite difference method, the following condition must be respected[**?**]:

$$\delta t \leq \frac{(\delta x)^2}{2} \tag{21}$$

To discretize the derivatives, we use the Taylor series expansion up to the first degree for the point x_j forward and backward:

$$\begin{aligned} f(x_j+\delta x) &= f(x_j) + (x_j+\delta x - x_j)f'(x_j) \\ &= f(x_j) + \delta x f'(x_j), \\ f(x_j-\delta x) &= f(x_j) + (x_j-\delta x - x_j)f'(x_j) \\ &= f(x_j) - \delta x f'(x_j), \end{aligned} \tag{22}$$

if we subtract the second equation from the first and solve for $f'(x_j)$, we can find the "Central Differences" which we can also discretize as:

$$f'(x_j) = \frac{f(x_j+\delta x) - f(x_j-\delta x)}{2\delta x} = \frac{f_{j+1} - f_{j-1}}{2\delta x} \tag{23}$$

In this way, we can rewrite our system of equations, once the discretization and algebraic development of the matrix have been performed:

$$\phi_{A,j} + \frac{i\delta t}{2\hbar}(V_j\phi_{A,j} + (k_{\alpha-,j} + k_{\beta-,j})\,\phi_{B,j} - i\hbar v_{\text{F}}\frac{\phi_{B,j+1} - \phi_{B,j-1}}{2\delta x}) = 2\psi_{A,j} \tag{24}$$

$$\phi_{B,j} + \frac{i\delta t}{2\hbar}(V_j\phi_{B,j} + (k_{\alpha+,j} + k_{\beta+,j})\,\phi_{A,j} - i\hbar v_{\text{F}}\frac{\phi_{A,j+1} - \phi_{A,j-1}}{2\delta x}) = 2\psi_{B,j} \tag{25}$$

If we add equations eq.(24) and eq.(25):

$$2\begin{pmatrix}\psi_{A,1}+\psi_{B,1}\\ \psi_{A,2}+\psi_{B,2}\\ \vdots\\ \psi_{A,J}+\psi_{B,J}\end{pmatrix}=\begin{pmatrix}N & Q & 0 & \dots & \dots & \dots & 0\\ -Q & N & Q & 0 & \dots & \dots & 0\\ 0 & -Q & N & Q & 0 & \dots & 0\\ \vdots & 0 & -Q & N & Q & \ddots & 0\\ \vdots & \vdots & 0 & -Q & N & \ddots & 0\\ \vdots & \vdots & \vdots & \ddots & \ddots & \ddots & Q\\ 0 & 0 & 0 & 0 & 0 & -Q & N\end{pmatrix}\begin{pmatrix}\phi_{A,1}\\ \phi_{A,2}\\ \vdots\\ \phi_{A,J}\end{pmatrix} \tag{26}$$

$$+\begin{pmatrix}M & Q & 0 & \dots & \dots & \dots & 0\\ -Q & M & Q & 0 & \dots & \dots & 0\\ 0 & -Q & M & Q & 0 & \dots & 0\\ \vdots & 0 & -Q & M & Q & \ddots & 0\\ \vdots & \vdots & 0 & -Q & M & \ddots & 0\\ \vdots & \vdots & \vdots & \ddots & \ddots & \ddots & Q\\ 0 & 0 & 0 & 0 & 0 & -Q & M\end{pmatrix}\begin{pmatrix}\phi_{B,1}\\ \phi_{B,2}\\ \vdots\\ \phi_{B,J}\end{pmatrix} \tag{27}$$

Where $N = 1 + \frac{i\delta t}{2\hbar}\left(V_j + (k_{\alpha+,j} + k_{\beta+,j})\right)$, $Q = \frac{i\hbar v_{\mathrm{F}}}{2\delta x}$ and $M = 1 + \frac{i\delta t}{2\hbar}\left(V_j + (k_{\alpha-,j} + k_{\beta-,j})\right)$.

As can be seen, the size of the matrix depends on the size of our system. If we choose $\delta x = 1$Å, then a quantum well of 1200Å will generate a matrix of 1200×1200.

We repeat the previous procedure but now subtracting equations eq.(24) and eq.(25)

Looking at these matrices, we can redefine them as two simple matrix equations $2\psi_+ = \mathbb{N}\phi_A + \mathbb{M}\phi_B$ and $2\psi_- = \mathbb{L}\phi_A + \mathbb{P}\phi_B$. These equations can be treated as a system of matrix equations that are solved as follows:

$$\begin{aligned}\phi_A &= (2\mathbb{N}^{-1})\psi_+ - (\mathbb{N}^{-1}\mathbb{M})\phi_B\\ \phi_B &= 2(-\mathbb{L}\mathbb{N}^{-1}\mathbb{M} + \mathbb{P})^{-1}(\psi_- - \mathbb{L}\mathbb{N}^{-1}\psi_+)\end{aligned} \tag{28}$$

Once we have the discretized system of equations, the temporal evolution can be calculated with:

$$\Psi_j^{n+1} = \Phi_j^n - \Psi_j^n \tag{29}$$

Repeating the process for each n until reaching N.

E. Probability Current Density

Once we have the temporal evolution, we can calculate its transmission coefficient from the calculation of the probability current density (PCD). To find this current, we start from the following continuity equation:

$$\frac{\partial \rho}{\partial t} + \nabla \cdot \vec{j} = 0 \tag{30}$$

Applying the conjugate transpose to the time-dependent Schrödinger equation(12), and multiplying on the right by Ψ, we can incorporate the probability density equation(16). At the same time, we consider the graphene Hamiltonian(1), which we know is Hermitian since it is composed of Pauli matrices. In this way, we can construct the following equation:

$$\frac{\partial}{\partial t}\int \rho d\vec{r} = -v_f \int \left(\Psi\vec{\sigma}\cdot\nabla\Psi^{T*} + \Psi^{T*}\vec{\sigma}\cdot\nabla\Psi\right) d\vec{r} \tag{31}$$

We can rewrite the equation by factoring out ∇ and removing the integral from both sides:

$$\frac{\partial}{\partial t}\rho = -v_f \nabla \cdot \left(\Psi^\dagger \vec{\sigma}\Psi\right) \tag{32}$$

Substituting into the continuity equation of probability density eq.(30):

$$\nabla \cdot \vec{j} = v_f \nabla \cdot \left(\Psi^\dagger \vec{\sigma}\Psi\right) \tag{33}$$

Eliminating ∇ from both sides:

$$\vec{j} = v_f \Psi^\dagger \vec{\sigma}\Psi \tag{34}$$

In this way, we have obtained the probability current density in graphene.

If we want to obtain the components of the current density, we can do it as follows:

$$\vec{j} = v_f \begin{pmatrix}\Psi^\dagger\sigma_x\Psi\\ \Psi^\dagger\sigma_y\Psi\end{pmatrix} = v_f \begin{pmatrix}\Psi_A^\dagger\Psi_B + \Psi_B^\dagger\Psi_A\\ i(-\Psi_A^\dagger\Psi_B + \Psi_B^\dagger\Psi_A)\end{pmatrix} \tag{35}$$

The importance of the current vector expression, shown explicitly in equation(35), lies in the detailed understanding of the pseudospin behavior of graphene. The clear

characterization of both components of the current vector is central to interpreting the numerical results and understanding the phenomenology associated with transport in these structures.

As a verification, if we consider an incident plane wave function, we can express it as:

$$\Psi(\vec{r}) = \frac{e^{i\vec{k}\cdot\vec{r}}}{\sqrt{2}} \begin{pmatrix} 1 \\ e^{i\theta} \end{pmatrix}, \tag{36}$$

where θ is the angle of incidence with respect to the direction normal to the barrier and $\vec{k} = k(\cos\theta, \sin\theta)$ is the wave vector.

If we substitute eq.(36) into eq.(35), we can simply perform the multiplication as follows to obtain the probability current density incident on the barrier along the X axis ($j_{x,in}$):

$$\begin{aligned} j_{x,in} &= v_f \frac{1}{2} \begin{pmatrix} e^{-i\theta} & 1 \end{pmatrix} \begin{pmatrix} 0 & 1 \\ 1 & 0 \end{pmatrix} \begin{pmatrix} 1 \\ e^{i\theta} \end{pmatrix} \\ &= v_f \left(\frac{e^{-i\theta} + e^{i\theta}}{2} \right) \\ &= v_f \cos\theta \end{aligned} \tag{37}$$

This simplification is what is commonly used in the literature[**? ?**].

To determine the numerical value of $\vec{j}$, we identify the peaks in the probability density plots. Subsequently, we calculate the minima of the Gaussian curves to find the apparent width of the GWP. Finally, we locate two precise moments: immediately before the wave packet interacts with the potential barrier and the exact moment it has traversed the barrier.

With the defined entry (t_1) and exit (t_2) times, we use equation eq.(35) for the entire space at each of these times.

With this, we can now calculate the transmission coefficient:

$$T = \left| \frac{\vec{j}_{out} \cdot \hat{n}}{\vec{j}_{in} \cdot \hat{n}} \right|, \tag{38}$$

In this context, the ratio between the transmitted current and the incident current is calculated, considering the product with the vector normal to the barrier. In the one-dimensional case addressed here, this vector can be represented as $(1, 0)$ or $(0, 1)$, depending on whether the Gaussian wave packet (GWP) propagates along the x-axis or the y-axis, respectively.

Having presented the conceptual framework and the fundamental equations of the studied system, we now proceed with the analysis and critical discussion of the results obtained through numerical simulations. This section will allow us to evaluate and contrast in detail the influence of the Rashba term on quantum transmission in monolayer graphene.

III. DISCUSSION OF RESULTS

A continuación se muestran las figuras obtenidas con el procedimiento obtenido anteriormente.

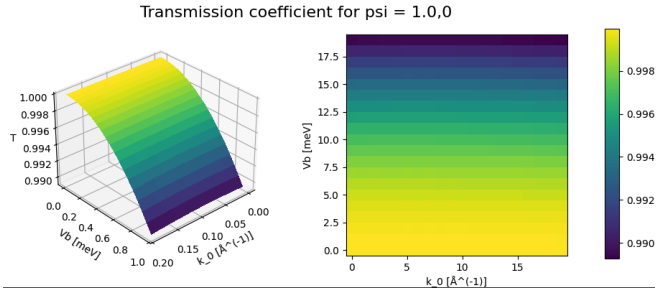

FIG. 1. figure

Transmission coefficient (T) in pristine graphene with initial pseudospinor configuration $\xi = (1, 0)$, plotted against potential barrier height (V_b, in meV) and initial wave vector (k_0, in Å^{-1}). The 3D plot and 2D heatmap show that transmission is largely independent of the initial wave vector but decreases noticeably as the barrier height increases, ranging from 1 to approximately 0.990.

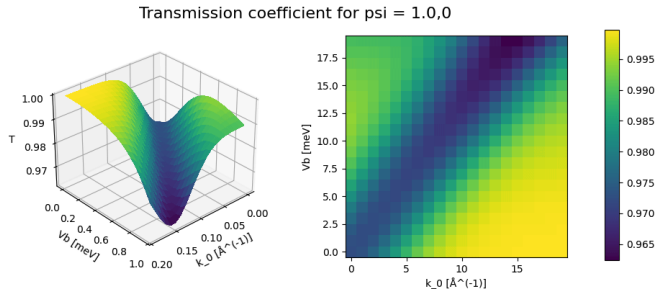

FIG. 2. figure

Coeficiente de transmisión (T) en función de la altura de la barrera de potencial (V_b) y el número de onda inicial (k_0) con una configuración inicial de pseudoespinor $\xi = (1, 0)$. La superficie 3D y el mapa de color 2D muestran una dependencia no monotónica de T con respecto a V_b y k_0, destacando la influencia del acoplamiento espín-órbita en la transmisión a través de la barrera.

En las imágenes podemos notar ciertos aspectos interesantes, empezando con la fig.1. La imagen presenta dos gráficos que ilustran el coeficiente de transmisión (T) en función de Vb (en meV) y k_0 (en Å^{-1}) para un valor fijo de $\xi = (1, 0)$. El gráfico de la izquierda es una visualización tridimensional donde T está en el eje z, Vb en el eje x y k_0 en el eje y, con una escala de colores que varía desde morado oscuro (menor T) hasta amarillo brillante (mayor T). El gráfico de la derecha es un mapa de calor bidimensional que ofrece una vista superior, con el eje x representando k_0 y el eje y representando Vb, usando el mismo mapa de colores que el gráfico 3D. Ambos gráficos muestran que el coeficiente de transmisión generalmente se mantiene muy cerca de 1, indicando una alta transmisión. Conforme aumenta Vb, T tiende a disminuir, mientras que la dependencia respecto a k_0 es mínima.

En general, los gráficos demuestran cómo cambia T con variaciones en Vb y k_0, destacando una leve disminución de T al aumentar Vb y un cambio insignificante respecto a k_0.

Este resultado muestra una contradicción con lo que ya se especifíca en la literatura, en el grafeno se esperaría observar una transmisión total debido a las mismas propiedades del material[**?** **?**].

Estas diferencias observadas pueden atribuirse principalmente a los siguientes aspectos relacionados con nuestro método y condiciones de simulación:

- Wave Packet Characteristics: Nuestra simulación utiliza un paquete de onda (GWP) compuesto por múltiples autoestados de momentum en lugar de considerar un único estado propio. Esta elección implica contribuciones simultáneas de varios estados, que potencialmente generan interferencias cuánticas afectando ligeramente el coeficiente de transmisión[**?**]. Este punto, resaltado por nuestra modelación dinámica en tiempo, marca una diferencia significativa respecto a los modelos teóricos ideales donde dichas interferencias no aparecen.

  Además, nuestra simulación contempla explícitamente la variable tiempo, algo poco frecuente en estudios teóricos previos ideales y estáticos. Investigar cómo estos aspectos dinámicos, como el tiempo de fase o el tiempo de túnel, afectan específicamente la transmisión observada es un objetivo importante propuesto para trabajos posteriores.

- Efectos de interferencia cuántica por dispersión del paquete en el tiempo: Como ha sido sugerido por la literatura[**?**], al evolucionar temporalmente un paquete de onda gaussiano suficientemente ancho, este se dispersa espacialmente de tal forma que diferentes partes del mismo interactúan simultáneamente con la barrera, causando interferencias internas consigo mismas. Tal interferencia es una posible causa adicional de las fluctuaciones en la transmisión observada en nuestros resultados numéricos.

Estos puntos explican las diferencias encontradas claramente desde una perspectiva metodológica y vinculan nuestros resultados numéricos respecto a la predicción teórica mencionada en los estudios previos. Esto no solo aclara la aparente contradicción, sino que también permite reforzar claramente el vínculo entre nuestros resultados específicos y el objetivo principal de analizar efectos dinámicos y propiedades que surgen al emplear paquetes de onda Gaussianos en simulaciones de tunneling cuántico en sistemas basados en grafeno.

Por otro lado, tenemos la transmisión bajo presencia de SOIR (Fig.2).

Se observa una correlación entre las variables: generalmente, a mayor altura de la barrera de potencial (Vb) y mayor número de onda inicial (k_0), se espera una menor transmisión. Sin embargo, la interacción espín-órbita introduce un comportamiento más complejo. A medida que k_0 aumenta y Vb disminuye, la transmisión se acerca a 1, indicando una mayor probabilidad de tunelamiento cuántico debido a la SOIR.

Aunque la variación en el coeficiente de transmisión es pequeña (del orden de 10^{-2}), es significativa y atribuible a la interacción SOIR. Los electrones, con sus diferentes componentes de pseudoespín, interactúan, y esta interacción se ve afectada por el número de onda inicial del paquete de ondas gaussiano (GWP), como se observó en estudios previos[**?**]. Por lo tanto, la SOIR modula la interacción, lo que a su vez causa las fluctuaciones observadas en el coeficiente de transmisión.

Es importante destacar aquí que la obtención analítica del vector corriente (ec. 35) ha sido determinante para interpretar los resultados obtenidos numéricamente. En particular, esta ecuación permite vincular explícitamente diferencias observadas en los coeficientes de transmisión con los componentes pseudoespinoriales y sus correlaciones cruzadas debido a la interacción Rashba. Por lo tanto, este resultado no solo brinda claridad conceptual, sino que también sienta las bases para futuras investigaciones teóricas y experimentales sobre transporte spintrónico avanzado en grafeno.

Tras analizar exhaustivamente los resultados numéricos y discutir los aspectos particulares observados en los coeficientes de transmisión electrónica con y sin interacción Rashba, podemos sintetizar a continuación las principales conclusiones alcanzadas en este trabajo, resaltando sus implicaciones teóricas y tecnológicas, así como las perspectivas para futuros estudios y aplicaciones.

IV. CONCLUSIONS

In this work, we explored the effect of Rashba spin-orbit interaction (SOIR) on electronic transmission through a potential barrier in monolayer graphene using numerical simulations based on Gaussian wave packets and finite difference methods (FDM). The results revealed how the presence of the Rashba term introduces substantial and complex modifications to the transmission coefficients compared to the simple behavior observed in pristine graphene. These variations originate from spin-dependent scattering mechanisms, such as spin degeneracy lifting and quantum interferences derived from the multiple components of the wave packets used in our simulations.

Regarding the questions initially posed in this study, we successfully demonstrated that SOIR interactions do significantly modify transmission characteristics, thus affirmatively answering our initial inquiries. Additionally, we clarified that small deviations observed in pristine graphene from the theoretical unitary transmission are a direct consequence of the nature of the Gaussian packets employed, emphasizing the importance of considering these effects in simulations and practical applications.

Collectively, our findings clearly highlight that a detailed understanding of SOIR provides predictive capability and essential tools for the engineering of spintronic

devices and platforms applicable to quantum computing. Therefore, this study firmly reaffirms the relevance of these fundamental quantum phenomena in current and future technological scenarios.

- E. Serna, I. R. Vargas, R. Pérez-Álvarez, and L. D. Cisneros, J. Appl. Phys. **125**, 203902 (2019).
- W. E. Liu, E. M. Hankiewicz, and D. Culcer, Materials **10**, 7 (2017).
- A. Avsar, J. Y. Tan, T. Taychatanapat, J. Balakrishnan, G. K. W. Koon, Y. Yeo, J. Lahiri, A. Carvalho, A. S. Rodin, E. C. T. O'Farrell, G. Eda, A. H. C. Neto, and B. Özyilmaz, Nat. Commun. **5**, 4875 (2014).
- H. Liu, H. Wang, Z. Peng, J. Jin, Z. Wang, K. Peng, W. Wang, Y. Xu, Y. Wang, Z. Wei, D. Zhang, Y. J. Li, W. Chu, and L. Sun, Nanoscale Horiz. **8**, 1235 (2023).
- E. B. Sonin, Phys. Rev. B. **79**, 19 (2009).
- L. Dell'Anna, P. Majari, and M. R. Setare, J. Phys.: Condens. Matter **30**, 415301 (2018).
- B. Trauzettel, D. V. Bulaev, D. Loss, and G. Burkard, Nat. Phys. **3**, 192 (2007).
- A. E. Bernardini, J. Phys. A.: Math. Theor. **43**, 489801 (2010).
- E. Paredes-Rocha, Y. Betancur-Ocampo, N. Szpak, and T. Stegmann, Phys. Rev. B. **103**, 045404 (2021).
- Y. Avishai and Y. B. Band, Phys. Rev. B. **104**, 075414 (2021).
- D. Shcherbakov, P. Stepanov, and et. al., Sci. Adv. **7**, 5 (2021).
- F. Delkhosh and A. Phirouznia, Physica E. **66**, 252 (2015).
- Z. Wang, D.-K. Ki, J. Y. Khoo, D. Mauro, H. Berger, L. S. Levitov, and A. F. Morpurgo, Phys. Rev. X **6**, 041020 (2016).
- Y. Gindikin and A. Kamenev, Phys. Rev. B **111**, 035104 (2025).
- Y.-T. Yao, S.-Y. Xu, and T.-R. Chang, Mater. Horiz. **11**, 3420 (2024).
- A. K. Geim and K. S. Novoselov, Nature Mater. **6**, 183 (2007).
- R. Cuan and L. Diago-Cisneros, Rev. Cub. Fís. **27**, 212 (2010).
- R. Cuan and L. Diago-Cisneros, EPL **110**, 67001 (2015).
- A. W. López, *Acoplamiento Espín-Órbita en Heteroestructuras Semiconductoras*, Master's thesis, Universidad Nacional Autónoma de México (2005).
- B. Hunt, J. Sanchez-Yamagishi, A. Young, M. Yankowitz, B. LeRoy, K. Watanabe, T. Taniguchi, P. Moon, M. Koshino, P. Jarillo-Herrero, and R. Ashoor, Science **340**, 1427 (2013).
- M. S. Fuhrer, Science **340**, 1413 (2013).
- P. Palla, G. R. Uppu, A. S. Ethiraj, and J. P. Raina, Bull. Mater. Sci. **39**, 1441 (2016).
- A. Carrillo and O. Mendoza, Geofísica UNAM (2015).
- D. Dahal and G. Gumbs, J. Phys. Chem. Solids **100**, 83 (2017).
- Z. Wu, K. Chang, J. T. Liu, X. J. Li, and K. S. Chan, J. Appl. Phys. **105**, 043702 (2009).
- D. W. Horsell, F. V. Tikhonenko, R. V. Gorbachev, and A. K. Savchenko, Phil. Trans. R. Soc. A **366**, 245 (2008).
- A. F. Young and P. Kim, Nature Phys **5**, 222 (2009).
- M. Staelens and F. Marsiglio, Am. J. Phys. **89**, 693 (2021).
- A. Molgado, O. Morales, and J. A. Vallejo, Rev. Mex. Fis. E **64**, 1 (2018).